Cerebral Hemoglobin and Optical Pathlength Influence Near-Infrared Spectroscopy Measurement of Cerebral Oxygen Saturation

C. Dean Kurth, MD, and Brian Uher, BS

Department of Anesthesiology and Critical Care Medicine, Children's Hospital of Philadelphia, and Departments of Anesthesia, Physiology, and Pediatrics, University of Pennsylvania School of Medicine, Philadelphia, Pennsylvania

Near-infrared spectroscopy (NIRS) is a noninvasive optical technique to monitor cerebral oxygen saturation at the bedside. Despite its applicability, NIRS has had limited clinical use because of concerns about accuracy, noted by intersubject variability in slope and intercept of the line between NIRS- and weighted-average arterial-cerebrovenous saturation (SmO_2). This study evaluated transcranial optical pathlength and cerebral hemoglobin concentration as sources for this intersubject variability. Experiments were performed in an *in vitro* brain model and in piglets. Optical pathlength and cerebral hemoglobin concentration were measured by time-resolved spectroscopy (TRS). NIRS and TRS were recorded in the model, as perfusate blood saturation was varied (0%–100%) at several hemoglobin concentrations, and in piglets, as SmO_2 was varied (15%–90%) before and after hemodilution. In the model, hemoglobin concentration significantly altered the NIRS versus blood saturation line slope and intercept, as well as optical pathlength. In piglets (before hemodilution), there was significant intersubject variability in NIRS versus SmO_2 line slope (0.73–1.4) and intercept (−24 to 36) and in transcranial optical pathlength (13.4–16 cm) and cerebral hemoglobin concentration (0.58–1.1 g/dL). By adjusting the NIRS algorithm with optical pathlength or cerebral hemoglobin measurements, intersubject variability in slope (0.9–1.2) and intercept (−9 to 18) decreased significantly. Hemodilution significantly changed NIRS versus SmO_2 line slope and intercept, as well as transcranial optical pathlength and cerebral hemoglobin concentration (before versus after hemodilution: slope 0.9 vs 0.78, intercept 13 vs 19, pathlength 13.9 vs 15.6 cm, cerebral hemoglobin 0.98 vs 0.73 g/dL). By adjusting the NIRS algorithm with the cerebral hemoglobin measurements, slope and intercept remained unchanged by hemodilution. These data indicate that intersubject variability in NIRS originates, in part, from biologic variations in transcranial optical pathlength and cerebral hemoglobin concentration. Instruments to account for these factors may improve NIRS cerebral oxygen saturation measurements.

(Anesth Analg 1997;84:1297–305)

Near-infrared spectroscopy (NIRS) is a noninvasive optical method for the bedside monitoring of cerebral oxygenation that has been used to investigate cerebral oxygen dynamics during pediatric and adult cardiac surgery (1,2), carotid endarterectomy (3,4), and neonatal resuscitation (5,6). The method relies on the relative transparency of the biologic tissues to near-infrared light (700–900 nm), in which oxy- and deoxyhemoglobin have distinct absorption spectra. By monitoring the absorption of light at several wavelengths in the near-infrared range, it is possible to monitor brain tissue concentrations of oxy- and deoxyhemoglobin, total hemoglobin, and hemoglobin oxygen saturation (6–8). NIRS differs from pulse oximetry in several respects. NIRS monitors a tissue field beneath the sensor, which contains capillaries, arteries, and veins; therefore, NIRS oxygen saturation represents a mixed vascular saturation dominated by small, gas-exchanging vessels. NIRS reflects oxygen extraction by tissue in response to changes in cerebral blood flow, arterial saturation and hematocrit, and cerebral oxygen metabolism (1,2,7,9). In contrast, pulse oximetry is influenced mainly by cardiopulmonary factors and reflects only arterial saturation.

Despite its applicability, NIRS has had limited clinical use because of concerns about its accuracy. Complicating the validation of NIRS has been the lack of a standard for comparison. Pollard and colleagues (10,11) used arterial-jugular bulb-weighted average

This research was supported in part by National Institutes of Health Contracts N43-NS-4-2314 and NO1-NS-1-2315.

Accepted for publication February 2, 1997.

Address correspondence and reprint requests to C. Dean Kurth, MD, Department of Anesthesiology, Children's Hospital of Philadelphia, 34th and Civic Center Blvd., Philadelphia, PA 19104. Address e-mail to Kurth@email.CHOP.edu.

©1997 by the International Anesthesia Research Society
0003-2999/97/$5.00

saturation to validate NIRS oxygen saturation. Because NIRS oxygen saturation originates from within a field containing capillaries, arteries, and veins, it can be estimated from the combined saturation of arterial and venous blood calculated in proportion to their contribution to cerebral blood volume (approximately 25% arterial, 75% venous) (12). During graded hypoxia in human volunteers, they observed good correlations between NIRS and weighted-average saturation, although slopes and intercepts were not homogenous among the volunteers and agreement between the measures was often imprecise (10,11). Wide intersubject variability in slope and intercept has also been observed by other investigators in humans (13) and in animals (7).

The source of intersubject variability and apparent inaccuracy in NIRS oxygen saturation measurements has not been examined. However, in the derivation of oxygen saturation, NIRS makes several assumptions involving optical pathlength and hemoglobin concentration in the tissue field, which suggests that these factors might be a source of intersubject variability. In this study, the mathematical relationship among NIRS oxygen saturation, optical pathlength, and hemoglobin concentration is described, and the effect of optical pathlength and hemoglobin concentration on NIRS oxygen saturation measurements are examined experimentally in an *in vitro* model of the brain and *in vivo* in piglets.

Methods

Theory

NIRS relies on a modification of the Beer-Lambert law to derive cerebral oxygen saturation from light absorption differences between wavelengths to yield an expression

$$G = LHk(Sco_2) + LHk' \quad (1)$$

where G is measured light attenuation difference between wavelengths, H is brain tissue hemoglobin concentration, Sco_2 is cerebral oxygen saturation, and k and k′ are lump constants (see Appendix). Note that H represents hemoglobin mass per volume of brain tissue, which is distinct from blood hemoglobin concentration. Equation 1 demonstrates a linear relationship between G and Sco_2 as long as L and H remain constant. Historically, this relationship was solved empirically because it had not been possible to measure either L or H *in vivo.* However, it is evident that errors might occur if L and H are not constant between subjects or conditions (e.g., hemodilution).

Instrumentation

Cerebral oximeters by NIM Inc. (RunMan®; Philadelphia, PA) and Somanetics Inc. (Invos 3100®; Troy, MI) were used to determine Sco_2. Both instruments consist of a probe housing a near-infrared light source and photodiode detectors and a main unit connected to the probe by wire bundle. The Invos 3100® uses 730 and 810 nm light, and RunMan® uses 750 and 850 nm light. The light emitter-detector separation is 3 cm in the RunMan® probe and both 3 and 4 cm in the Invos 3100® probe. In RunMan®, optical density difference and Sco_2 are calculated by a computer connected to the main unit (14). In the Invos 3100®, the main unit houses the electronics to calculate Sco_2.

A time-resolved spectrophotometer (TRS; Hamamatsu Photonics, Hamamatsu, Japan) was used to determine optical pathlength and cerebral hemoglobin concentration (14–16). The instrument consists of two fiberoptic bundles connected to a main unit housing picosecond-pulsed lasers emitting at 780 and 830 nm, a time-gated multichannel photon detector, and a computer. One fiberoptic bundle conveys the laser light pulses from the main unit to the head, and the other fiberoptic bundle receives the light emerging from the head and conveys it to the time-gated detector. The computer calculates transcranial optical pathlength from the "time-of-flight" (t) of photons from emitter to detector by the relationship

$$L = ct/n \quad (2)$$

where c is the speed of light (30 cm/ns) and n is the refractive index of tissue (1.33). Transcranial optical pathlength was taken as the average of the 780- and 830-nm photon pathlengths. Cerebral hemoglobin concentration was determined from the absorption coefficients measured at 780 and 830 nm (14,17).

Blood oxygen saturation and hemoglobin concentration were measured by CO-Oximetry (Instrumentation Laboratory, Lexington, MA), and blood partial pressure of carbon dioxide (Pco_2) and oxygen (Po_2) and pH were measured by a blood gas analyzer (Corning Instruments, Corning, NY).

Brain Model Studies

The brain model is a solid plastic structure containing a microvascular network perfused with human blood equilibrated with O_2, N_2, and CO_2 in a closed circuit (14). The model's vascular volume comprises 5% of its total volume to simulate normal cerebral blood volume. Blood oxygen saturation is regulated by adjusting the flow of O_2 and N_2 in the circuit and measured by CO-Oximetry from an aliquot of blood. Hemoglobin concentration is regulated by adjusting the quantity of blood and diluent in the circuit.

The effect of hemoglobin concentration and optical pathlength on the relationship between optical density difference and oxygen saturation was determined as follows. Fiberoptic bundles from the TRS instrument and the RunMan® optical probe were placed against

the side of the model next to each another. Human packed red blood cells diluted with 0.9% saline were added to the circuit to achieve the desired hemoglobin concentration. Perfusate Pco_2 (40 torr), pH (7.40), and temperature (37°C) were held constant during all experiments. As perfusate oxygen saturation was increased from 0% to 100% in approximately 20% increments, optical pathlength and optical density difference were recorded. Experiments were performed with perfusate hemoglobin concentrations of 15 g/dL, 10 g/dL, and 7 g/dL. The effect of hemoglobin concentration on optical pathlength in the model was also determined with blood oxygen saturation held constant (100%). TRS optical fibers were positioned against the model as described above. As perfusate hemoglobin concentration was decreased from 15 g/dL to 6 g/dL in 3-g/dL steps, optical pathlength was recorded. Hemoglobin concentration in the brain model (equivalent to H in Equation 1) was calculated as 5% of perfusate hemoglobin concentration, which corresponds to the channel volume per total volume of the model.

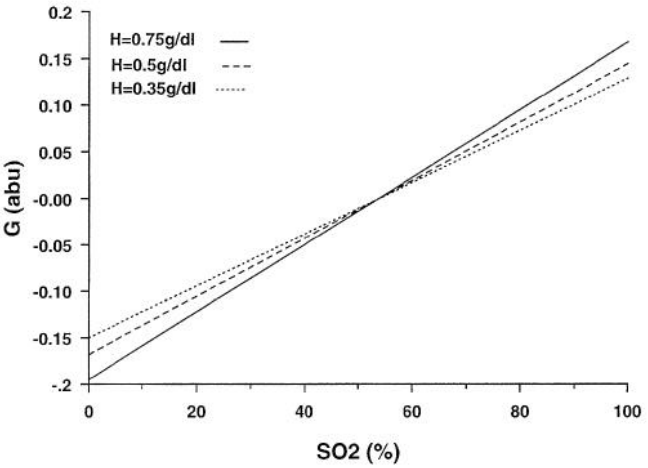

Figure 1. Effect of blood oxygen saturation (So_2) on differential light attenuation (G) at varying hemoglobin concentrations in the brain model (H) (see Equation 1, Methods). abu-absorbance units. Hemoglobin values represent 5% of the hemoglobin concentration in the model's vascular system. For H = 0.75 g/dL, y = 36x −20, $r^2 = 0.98$, $P < 0.001$; for H = 0.5 g/dL, y = 31x − 17, $r^2 = 0.97$, $P < 0.001$; and for H = 0.35 g/dL, y = 28x − 15, $r^2 = 0.99$, $P < 0.001$. Slope values were multiplied by 10^4 and intercept values were multiplied by 10^2. Slopes and intercepts differ significantly ($P < 0.01$) between the lines.

Piglet Studies

To evaluate the effect of hemoglobin concentration and optical pathlength on Sco_2 measured *in vivo*, six piglets (aged 2–5 days, body weight 1.45–2.0 kg) were studied. Piglet studies were approved by our institutional animal care and use committee. After intramuscular ketamine (33 mg/kg) and acepromazine (3.3 mg/kg) were administered, the trachea was cannulated, and the lungs were mechanically ventilated. Catheters were inserted into the femoral artery to measure arterial saturation (Sao_2), into the external jugular vein to administer drugs, and into the superior sagittal sinus to measure cerebrovenous oxygen saturation (Svo_2). Anesthesia was maintained with intravenous fentanyl (25 $\mu g/kg$ load, then 10 $\mu g \cdot kg^{-1} \cdot h^{-1}$), droperidol (250 $\mu g \cdot kg^{-1} \cdot h^{-1}$), and pancuronium (0.1 $\mu g \cdot kg^{-1} \cdot h^{-1}$). A RunMan® ($n = 5$) or Invos 3100® ($n = 1$) probe was set on the head (skin, scalp, and skull were intact) with the emitter and detector 1 cm lateral to and parallel with the sagittal suture. TRS fiberoptics were on the contralateral hemisphere mirroring RunMan®; TRS was not used with Invos 3100®. Weighted-average cerebral oxygen saturation (Smo_2) was defined by

$$Smo_2 = 0.75(Svo_2) + 0.25(Sao_2) \quad (3)$$

Inspired oxygen concentration and ventilatory rate were adjusted to force Svo_2 over a wide range: normoxia (Svo_2 55%–70%), moderate hypoxia (Svo_2 35%–45%), severe hypoxia (Svo_2 15%–25%), and hypercapnia (Svo_2 80%–95%). The order was selected at random. All piglets experienced each condition; normoxia was experienced twice. NIRS, TRS, and CO-Oximetry were recorded at each condition. The experiment was then repeated after isovolemic hemodilution with lactated Ringer's solution to decrease arterial hemoglobin concentration by approximately 3 g/dL. At the end of the experiment, animals were killed with intravenous pentobarbital (100 mg/kg).

Statistical Analysis

Data are expressed as means ± SD or as ranges. NIRS Sco_2 and Smo_2 were compared by using regression tests, difference tests [Bland-Altman (18)], and split tests. Linear relationships were determined by least squares regression. Comparisons among animals or conditions were made by using analysis of variance. Bias and precision were defined as the mean ± 2 SD of, respectively, the ordinate for $Snirso_2 - Smo_2$ versus $(Snirso_2 + Smo_2)/2$. Homogeneity of the slopes, intercepts, and bias among piglets was assessed by analysis of covariance. The split test was the number of times NIRS Sco_2 "split" between arterial and cerebrovenous saturation. Significance was $P < 0.05$.

Results

In the brain model, linear relationships were observed between G and So_2 (Figure 1), consistent with Equation 1. Positive slope and negative intercept values reflect positive and negative values for k and k′, respectively. When the hemoglobin concentration in the brain model was decreased, the slope decreased ($P < 0.001$) and the intercept increased ($P < 0.001$), which

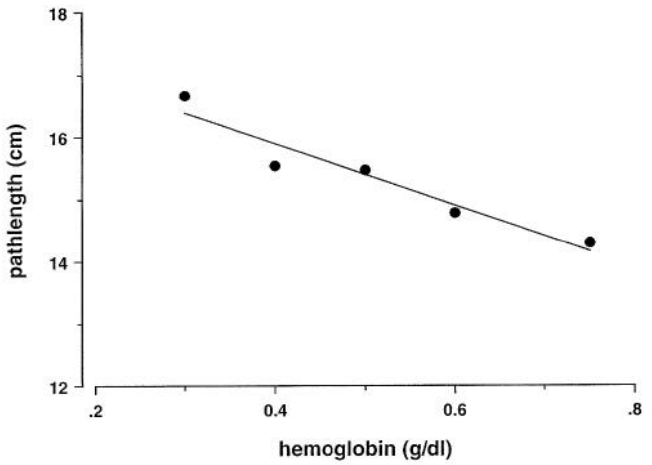

Figure 2. Effect of hemoglobin concentration on optical pathlength in the brain model (see Equation 1, Methods). $y = -4.9x + 17.9$, $r^2 = 0.92$, $P < 0.001$.

is also consistent with Equation 1. The inflection point of the three lines occurred at $So_2 = 55\%$, which indicates that as hemoglobin concentration decreases, NIRS underestimates Sco_2 above the inflection point and overestimates it below the inflection point.

In the brain model, optical pathlength was inversely related to perfusate hemoglobin concentration. During variable oxygen saturation, optical pathlength measured at the perfusate hemoglobin concentration 7 g/dL (14.3 ± 0.3 cm) was significantly greater than those at 10 g/dL (15.4 ± 0.2 cm) and 15 g/dL (17.2 ± 0.1 cm). During constant oxygen saturation, optical pathlength decreased linearly as perfusate hemoglobin concentration was decreased (Figure 2).

In piglets, linear relationships were observed between RunMan® oxygen saturation and Smo_2 (Table 1, Figure 3). Among animals, slopes ranged from 0.73 to 1.4, intercepts from 36 to −24, bias from −20% to 11%, and precision from 3% to 12%. There was significant interanimal variability (e.g., Piglet 1 versus Piglet 5) for slope ($P < 0.001$), intercept ($P < 0.001$), and bias ($P < 0.05$). In the split test, RunMan® oxygen saturation did split arterial and cerebrovenous saturation in 19 of 25 comparisons (76%) and failed to split in 6 of 25 (24%). Among animals, transcranial optical pathlength ranged from 13.4 to 16.0 cm, and cerebral hemoglobin concentration ranged from 0.58 to 1.10 g/dL (Table 2). There was significant interanimal variability in transcranial optical pathlength ($P < 0.001$), arterial hemoglobin concentration ($P < 0.05$), and cerebral hemoglobin concentration ($P < 0.01$).

Several biologic factors were examined as sources for the interanimal variability of the RunMan® Sco_2 versus Smo_2 line (Table 3). Of the factors, only transcranial optical pathlength and cerebral hemoglobin concentration were significantly correlated with the slope and the intercept of the lines, in that animals with greater slope and lesser intercept had greater transcranial optical pathlength and cerebral hemoglobin concentration. Significant correlation was also observed between transcranial optical pathlength and cerebral hemoglobin concentration ($r^2 = 0.70$, $P = 0.03$).

To determine whether the optical pathlength or cerebral hemoglobin measurements could be used to improve NIRS accuracy, the algorithm (Equation 1) was adjusted in each animal by stepwise linear regression with the optical pathlength and/or cerebral hemoglobin concentration measurements (Table 4). When the data from all animals were combined and analyzed, the adjusted algorithms had slopes and intercepts closer to unity and zero, respectively, and improved precision compared with the unadjusted algorithm. When the animals' data were analyzed individually, the range among animals in slope, intercept, and precision was decreased for the adjusted algorithms. However, significant interanimal variability persisted, and there continued to be occasions on which RunMan® Sco_2 did not split arterial and cerebrovenous saturation: 20% (5 of 20) for the pathlength adjusted algorithm, 16% (4 of 25) for the cerebral hemoglobin-adjusted algorithm, and 20% (5 of 25) for the pathlength-cerebral hemoglobin-adjusted algorithm.

The effect of acute hemodilution was examined on Sco_2 measurements with the RunMan® oximeter (Figure 4a; Table 5) and the Invos 3100® oximeter (Figure 4b). For both instruments, the slope of the NIRS oxygen saturation versus Smo_2 line was decreased ($P < 0.01$) and intercept was increased ($P < 0.01$) after hemodilution compared with before hemodilution. Hemodilution also increased transcranial optical pathlength (before versus after hemodilution: 13.9 ± 1.1 vs 15.6 ± 1.3 cm, $P < 0.05$) and decreased cerebral hemoglobin concentration (before versus after hemodilution: 0.98 ± 0.24 vs 0.73 ± 0.25 g/dL, $P < 0.05$). The slope, intercept, and pathlength changes with hemodilution are consistent with those seen with decreasing perfusate hemoglobin concentration in the brain model experiments.

To determine whether optical pathlength or cerebral hemoglobin concentration could be used to improve NIRS accuracy with hemodilution, the NIRS algorithm (Equation 1) was adjusted by stepwise linear regression with the measured pathlength and cerebral hemoglobin values before and after hemodilution (Table 5). In the pathlength-adjusted algorithm, there continued to be significant changes in the slope of the NIRS oxygen saturation versus Smo_2 line before versus after hemodilution. In the cerebral hemoglobin- and pathlength-cerebral hemoglobin-adjusted algorithms, slope and intercept remained unchanged. Hemodilution did not alter results of the difference or split tests for any of the algorithms.

Table 1. Comparison of Near-Infrared Spectroscopy and CO-Oximeter–Derived Cerebral Oxygen Saturation in Piglets

	Linear regression test[a]			Difference test[b]		Split test[c]
Pig	Slope	Intercept	r^2	Bias	Precision	Split
1	0.73	36	0.98	−20	6	4/5
2	0.75	19	0.96	−7	7	4/5
3	0.90	−6	0.81	11	11	3/5
4	0.92	13	0.99	−8	3	4/5
5	1.4	−24	0.95	0	12	4/5
All	0.94	7	0.71	−5	16	19/25

Values are mean or number.
[a] Linear regression is y = mx + b for RunMan® oxygen saturation (Sco_2) versus weighted-average arterial cerebral venous saturation (Smo_2).
[b] Difference test is Sco_2-Smo_2 versus (Sco_2 + Smo_2)/2 in which bias and precision are mean ± 2 SD of the ordinate.
[c] Split test is number of occasions Sco_2 fell between arterial and cerebral venous saturation of the total number of comparisons.

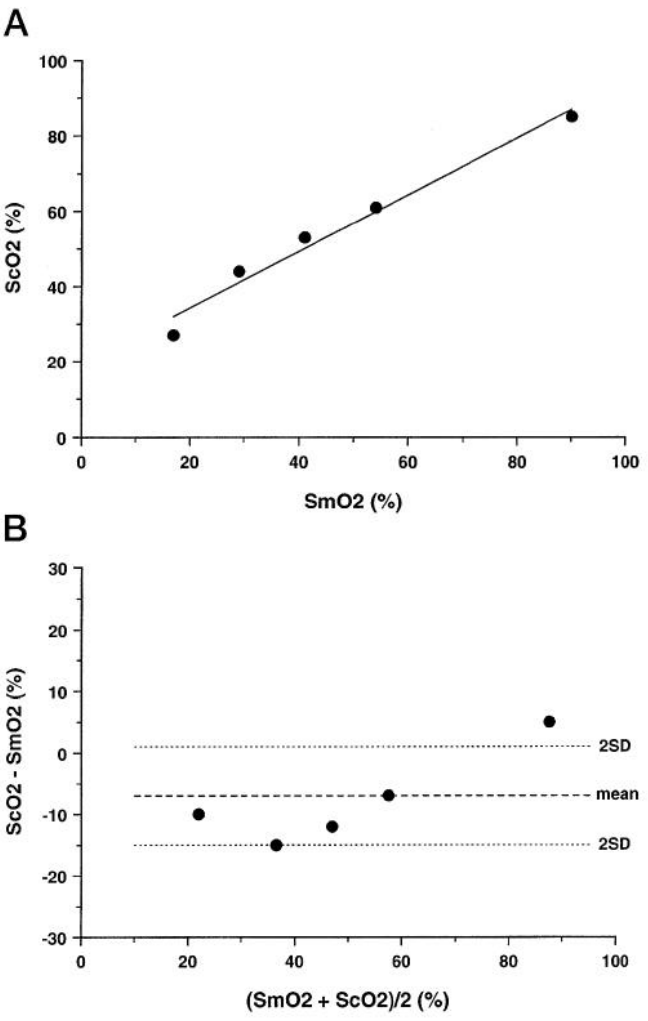

Figure 3. Representative comparisons of cerebral oxygen saturation as measured by near-infrared spectroscopy (Sco_2) with weighted-average arterial-cerebrovenous oxygen saturation (Smo_2) as measured by CO-Oximetry (Piglet 2, see Table 1). a, Linear regression test (y = 0.75x + 19, r^2 = 0.96, $P < 0.001$). b, Difference test. Lines depict bias ± precision.

Table 2. Transcranial Optical Pathlength and Hemoglobin Concentrations in Piglets

Pig	Pathlength (cm)	Arterial hemoglobin (g/dL)[a]	Cerebral hemoglobin (g/dL)[a]
1	13.4 ± 0.3	9.0 ± 0.2	0.58 ± 0.05
2	14.1 ± 0.3	9.0 ± 0.3	0.85 ± 0.19
3	14.2 ± 0.2	9.4 ± 0.2	0.94 ± 0.20
4	15.1 ± 0.2	11.1 ± 0.1	1.02 ± 0.18
5	16.0 ± 0.4	8.6 ± 0.2	1.10 ± 0.09
All	14.5 ± 0.8	9.4 ± 0.9	0.89 ± 0.20

Values are mean ± SD.
[a] Arterial and cerebral hemoglobin concentrations represent hemoglobin mass per volume of blood and brain tissue, respectively.

Table 3. Correlation Coefficients Between Piglet Factors and Slope and Intercept of the Line for Near-Infrared Spectroscopy Versus CO-Oximeter–Derived Cerebral Oxygen Saturation

	r^2
Slope versus	
Body weight	0.26
Postnatal age	0.47
Arterial hemoglobin	−0.23
Cerebral hemoglobin	0.78*
Transcranial optical pathlength	0.82*
Intercept versus	
Body weight	0.18
Postnatal age	−0.29
Arterial hemoglobin	0.20
Cerebral hemoglobin	−0.83*
Transcranial optical pathlength	−0.78*

* Significant correlation between piglet factor and slope or intercept ($P < 0.05$).

Discussion

NIRS is a noninvasive optical technique to monitor Sco_2 at the bedside. Despite its applicability, NIRS has had limited clinical use because of concerns about its accuracy, in that studies have reported that although NIRS and Smo_2 correlate well, interpatient variability exists in slope, intercept, and bias between the measures (10,11,13). In the present study, several lines of evidence indicate that intersubject variability originates, in part, from biologic variation in cerebral hemoglobin concentration and transcranial optical pathlength and its effect on the calculation of Sco_2 by the

Table 4. Comparison of Near-Infrared Spectroscopy and CO-Oximeter–Derived Cerebral Oxygen Saturation Using Several Near-Infrared Spectroscopy Algorithms in Piglets

	Near-infrared spectroscopy algorithm			
	No adjust[a]	Path adjust[a]	Heme adjust[a]	Path-heme adjust[a]
Regression test				
Slope	0.94 (0.7–1.4)	0.98 (0.8–1.1)*	0.99 (0.8–1.1)*	1.0 (0.9–1.2)*
Intercept	7 (−24 to 36)	4 (−15 to 24)*	4 (−6 to 21)*	3 (−9 to 18)*
r^2	0.71	0.74	0.77	0.78
Homogeneity	No	No	No	No
Difference test				
Bias	−5	−4	−6	0
Precision	16	12*	10*	12*
Homogeneity	No	No	No	No
Split test				
Split	19/25 (3/5–5/5)	20/25 (4/5–5/5)	21/25 (4/5–5/5)	20/25 (4/5–5/5)

Values are mean (range), $n = 5$. The mean represents data from all animals combined and analyzed as one. The range represents data from each animal analyzed individually.

[a] No adjust, path adjust, heme adjust, and path-heme adjust indicate that the algorithm was not adjusted for transcranial optical pathlength and cerebral hemoglobin concentration or that it was adjusted for pathlength, cerebral hemoglobin, or the combination, respectively.

* $P < 0.05$ versus no adjust value.

NIRS algorithm. First, in the brain model, hemoglobin concentration changed the NIRS versus blood oxygen saturation line slope and intercept and optical pathlength. Second, in piglets, NIRS versus SmO_2 line slope and intercept correlated with trancranial optical pathlength and cerebral hemoglobin concentration. By adjusting the NIRS algorithm with the optical pathlength and cerebral hemoglobin measurements in each animal, intersubject variability in slope and intercept decreased. Finally, acute hemodilution changed the NIRS versus SmO_2 line slope and intercept, as well as cerebral hemoglobin concentration and optical pathlength. By adjusting the NIRS algorithm with the cerebral hemoglobin concentration measurements, slope and intercept remained unchanged with hemodilution.

Lack of a gold standard for NIRS has complicated validation and identification of error sources. NIRS monitors a tissue field containing capillaries, arterioles, and venules, and its calculated oxygen saturation represents a mixed, microvascular oxygen saturation. No other method presently measures oxygen saturation in this region of the circulation. The brain model was developed as a means to better validate NIRS and identify error sources, because oxygen saturation and hemoglobin concentration in the model are known and can be varied independently. However, the brain model is limited by its simplicity and cannot replace biologic testing. Weighted-average oxygen saturation calculated from arterial and cerebral venous blood has been used to validate NIRS ScO_2 *in vivo* (10,11,14). However, it is an estimate that can introduce error because the ratio of arterial and venous blood may not be constant among subjects or conditions. The split test complements regression and differences tests because NIRS ScO_2 should always fall between arterial and venous saturation. In this study, we used the brain model, weighted-average estimate, and arterial-venous split to examine NIRS accuracy. These tests indicate that measurement errors do exist in certain subjects and during hemodilution and that variations in cerebral hemoglobin concentration and optical pathlength are sources of these errors.

NIRS include continuous wave instruments (cwNIRS), time-resolved instruments (trNIRS), and phase-modulated instruments (pmNIRS). cwNIRS has been available commercially for several years and uses incoherent light technology. RunMan® and Invos 3100® instruments are examples of cwNIRS. pmNIRS and trNIRS use coherent light technology and have the advantage of being able to measure optical pathlength as well as absorption (17). These instruments, however, remain under development, and their ScO_2 algorithms have not been tested. Previous work has found good correlation between cwNIRS and other measures of cerebral oxygen saturation (7,10,11,13,19). Pollard et al. (10–11) observed linear relationships between Invos 3100® and SmO_2 in adult humans, although wide intersubject variability in slope (0.4–1.3), intercept (−23 to 30), and bias (−8 to 8) was noted between the measures. In our study, intersubject variability between RunMan® and SmO_2 was similar to the findings of Pollard et al., even though different cwNIRS instruments were used and different species were studied. In addition, our results for the hemodilution experiments were similar for RunMan® and Invos 3100® instruments. These findings suggest that

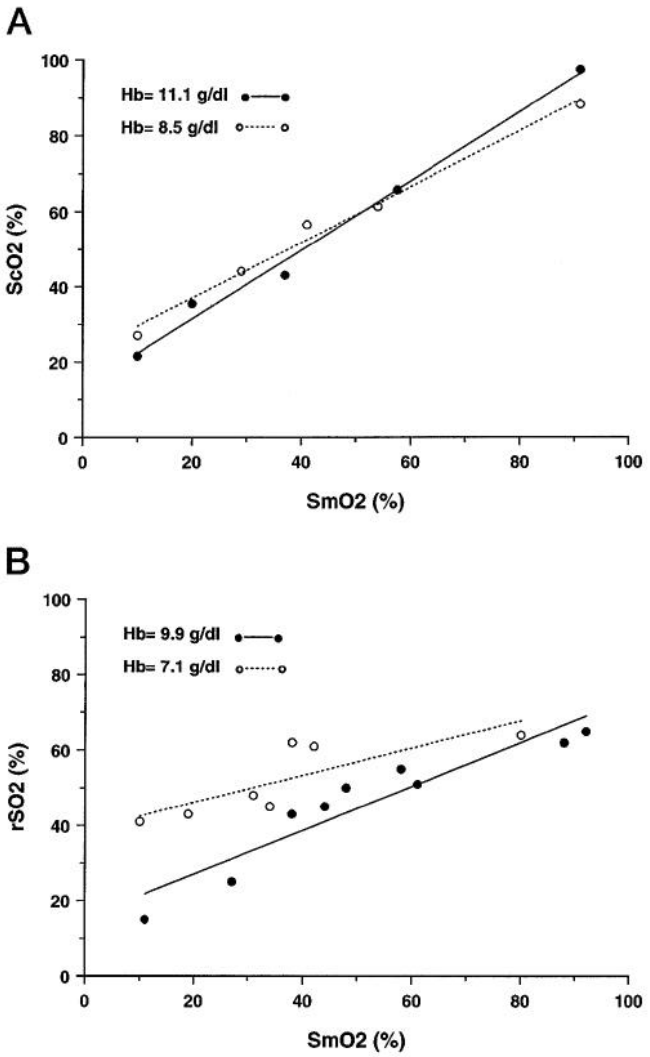

Figure 4. Effect of acute hemodilution on cerebral oxygen saturation measurements. Slopes and intercepts of the lines changed significantly before versus after hemodilution. Hb-blood hemoglobin concentration. a, RunMan® oximeter (Piglet 4, see Table 1). At Hb = 11.1 g/dL, y = 0.92x + 13, r^2 = 0.99. At Hb = 8.5 g/dL, y = 0.78x + 19, r^2 = 0.96. Slope and intercept comparison between lines, $P < 0.025$ and $P < 0.05$, respectively. b, Invos 3100® oximeter. At Hb = 9.9 g/dL, y = 0.58x + 15, r^2 = 0.88. At Hb = 7.1 g/dL, y = 0.36x + 38, r^2 = 0.72. Slope and intercept comparison between lines were $P < 0.005$.

intersubject variability originates in cwNIRS methodology, not the particular instrument, and reflects a limitation of cwNIRS technology.

Optical pathlength is an important factor in spectrophotometry through the Beer-Lambert law. In dilute, nonparticulate solutions, optical pathlength is the linear distance across the solution and is defined in benchtop spectrometers by the cuvette width (usually 1 cm). In particulate, highly scattering solutions such as tissue, optical pathlength is many times the linear distance across the solution. Computer simulations of optical paths in tissue describe photons traveling like pin balls deflecting off tissue particles (e.g., red blood cells, mitochondria) but roughly following an elliptical path between light emitter and detector (20). Photon pathlength is influenced by emitter-detector separation (wider separation, longer path), tissue light-scattering properties (higher scatter, longer path), and tissue absorbance (higher absorption, shorter path) (14,17,21,22). Optical pathlength is also influenced by tissue boundaries, which, in the head, include interfaces among scalp, skull, cerebrospinal fluid, and brain (23).

Until recently, optical pathlength in NIRS has been unknown. Advances in laser technology and electronics have now made it possible to measure optical pathlength by either trNIRS or frequency-resolved spectroscopy, which use the particle and wave properties of light, respectively (17). In the current study, optical pathlength was measured by trNIRS using the time-of-flight of photons, whereas in our previous studies, it was measured by frequency-resolved spectroscopy using a phase-shift of light waves (7,22). Both methods appear to yield similar optical pathlengths in piglets (7,22). Pathlength differences among subjects appears to arise from biologic variation in tissue light scattering, composition of tissue boundaries, and/or tissue absorption. The current study ties these biologic variations in optical pathlength to cwNIRS oxygen saturation measurement errors.

The current study also identified cerebral hemoglobin concentration as a factor that influences cwNIRS saturation. Although optical pathlength and hemoglobin concentration are independent variables in the cwNIRS algorithm (Equation 1), we did observe a significant relationship between them in both brain model and piglet experiments, consistent with the physics of light behavior in tissue (15,17,20). This relationship minimized the error in calculating saturation during hemodilution because the increase in transcranial optical pathlength partially offset the decrease in cerebral hemoglobin concentration to help maintain constancy of the slope (LHk) and intercept (LHk) in the algorithm. This relationship also explains why the pathlength-hemoglobin–adjusted algorithm did not substantially improve that of either pathlength or hemoglobin alone.

Several studies have suggested the applicability of cwNIRS to cardiac operations and carotid endarterectomy to monitor the brain (1–4,13). Cerebral hemoglobin concentrations may decrease during carotid artery occlusion (ischemia) and during cardiopulmonary bypass (hemodilution) (24,25). Our data reveal that cwNIRS overestimates Sco_2 when cerebral hemoglobin concentrations decrease, which suggests that during cardiac and cerebrovascular operations, these instruments may underestimate cerebral desaturation.

Table 5. Comparison of Near-Infrared Spectroscopy and CO-Oximeter–Derived Cerebral Oxygen Saturation Before Versus After Hemodilution Using Several Near-Infrared Spectroscopy Algorithms in Piglets

	Near-infrared spectroscopy algorithm							
	No adjust[a]		Path adjust[a]		Heme adjust[a]		Path-heme adjust[a]	
Linear regression test								
Slope	0.90	0.78*	0.83	0.69*	0.92	0.90	0.93	0.93
Intercept	13	19*	21	23	11	8	18	13*
Difference test								
Bias	−9	−10	−7	−9	−8	−3	−12	−5
Precision	3	6	3	8	4	4	5	5
Split test	11/15	11/15	13/15	13/15	13/15	13/15	13/15	13/15

Values are mean before (left) versus after (right) hemodilution for the RunMan® oximeter.
[a] No adjust, path adjust, heme adjust, and path-heme adjust indicate that the algorithm was not adjusted for transcranial optical pathlength and cerebral hemoglobin concentration or that it was adjusted for pathlength, cerebral hemoglobin, or the combination, respectively.
* $P < 0.05$ before versus after hemodilution.

The tissues overlying the brain can also influence the measurement of Sco_2, and this is an important issue in applying NIRS to adults (10,11,19,20,23). Because NIRS oxygen saturation originates from the illuminated volume of tissue beneath the probe, the measurement reflects the combined oxygen saturation of blood in the skin, scalp, skull, and brain. This illuminated tissue volume is determined by the absorbing and scattering properties of the tissue, the light emitter-detector separation on the NIRS probe, and the boundary conditions beneath the probe (17,20,23). Depending on the boundary condition, light may be back-scattered or piped forward, hindering or facilitating, respectively, brain measurements from the surface of the head. However, increasing emitter-detector separations on the NIRS probe illuminates deeper tissue regions to facilitate brain measurements (23). The present study did not examine the influence of overlying tissues on NIRS Sco_2 measurements, as the *in vitro* brain model did not simulate the head with multiple tissue boundaries, and the overlying tissues in piglets are thin and do not affect NIRS measurements (8,14).

Before NIRS can be used to manage patients, the accuracy of Sco_2 measurements should be improved, and the relationship between Sco_2 and brain injury should be defined better. By accounting for biologic variation in cerebral hemoglobin concentration and optical pathlength, cwNIRS accuracy can be increased. However, the approach of combining cwNIRS with a method to measure pathlength or cerebral hemoglobin concentration, such as trNIRS, was not entirely satisfactory. In addition, trNIRS is an expensive technology not easily used in the clinical environment. pmNIRS or spatially-resolved instruments may be able to account for these factors and measure Sco_2 more accurately (17). Further work is required to develop and validate these instruments for clinical use.

The authors thank Ms. Karen Nork for technical assistance in conducting these studies, Dr. Britton Chance for the use of the time-resolved spectrometer, Dr. W.T.M. Johnson for the use of the Somanetics Invos 3100® oximeter, and Dr. William Thayer for critically reviewing the manuscript.

Appendix

Transmission of light through tissue depends on a combination of absorption and scattering events that may be expressed as

$$G = A + S \quad \text{(a)}$$

where G is optical density of the tissue and A and S are absorption and scattering terms, respectively. G may also be defined in terms of light attenuation:

$$G = -f \log(I/I_o) \quad \text{(b)}$$

where I_o and I represent the intensities of the incident light on the tissue and of the detected light emerging from the tissue, respectively, measured by an instrument with a functionality constant, f. The absorption term, A, is related to the concentrations of oxyhemoglobin (HbO_2) and deoxyhemoglobin (Hb) through the Beer-Lambert law

$$A = \epsilon^{Hb}L(Hb) + \epsilon^{HbO_2}L(HbO_2) + A^0 \quad \text{(c)}$$

where ϵ^{Hb} and ϵ^{HbO_2} are the extinction coefficients of oxy- and deoxyhemoglobin, L is pathlength of the light through the tissue, and A^0 is absorption from substances other than hemoglobin in the tissue (e.g., water, cytochrome aa_3). Oxygen saturation (So_2) is

$$So_2 = HbO_2/H \quad \text{(d)}$$

in which H is total hemoglobin concentration

$$H = (Hb + HbO_2). \quad \text{(e)}$$

If light intensity is measured at 2 wavelengths, Equations a and c can be combined and expressed at each wavelength

$$G^1=\epsilon^{1Hb}L^1(Hb) + \epsilon^{1HbO_2}L^1(HbO_2)+A^1+S^1 \quad (f)$$

$$G^2=\epsilon^{2Hb}L^2(Hb) + \epsilon^{2HbO_2}L^2(HbO_2)+A^2+S^2 \quad (g)$$

where the superscripts 1 and 2 denote the values at wavelengths 1 and 2. If the wavelength pairs are chosen such that the extinctions coefficients of oxy- and deoxyhemoglobin differ, whereas optical pathlength, light scattering, and background absorption do not (i.e., $L^1 = L^2$, $S^1 = S^2$, and $A^1 = A^2$), Equations d–g can be solved simultaneously to yield Equation 3. k and k′ are lump constants for the extinction coefficients, represented as

$$k = \epsilon^{1Hb} + \epsilon^{2HbO_2} - \epsilon^{2Hb} - \epsilon^{1HbO_2} \quad (h)$$

$$k' = \epsilon^{2HbO_2} - \epsilon^{1Hb} \quad (i)$$

In the near-infrared spectrum between 750 and 850 nm, optical pathlength, light scattering, and background tissue absorption remain relatively constant, and it is possible to select wavelength pairs in which the extinctions of oxy- and deoxyhemoglobin differ (14,26–28).

References

1. Ausman JI, McCormick PW, Stewart M, et al. Cerebral oxygen metabolism during hypothermic circulatory arrest in humans. J Neurosurg 1993;79:810–5.
2. Kurth CD, Steven JM, Nicolson SC. Cerebral oxygenation during pediatric cardiac surgery using deep hypothermic circulatory arrest. Anesthesiology 1995;82:74–82.
3. Williams IM, Picton A, Farrell A, et al. Light-reflective cerebral oximetry and jugular bulb venous oxygen saturation during carotid endarterectomy. Br J Surg 1994;81:1291–5.
4. Kirkpatrick PJ, Smielewski P, Whitfield PC, et al. An observational study of near-infrared spectroscopy during carotid endarterectomy. Neurosurgery 1995;82:756–63.
5. Shah AR, Kurth CD, Gwiazdowski SG, et al. Fluctuations in cerebral oxygenation and blood volume during endotracheal suctioning in premature infants. J Pediatr 1992;120:769–74.
6. Wyatt JS, Delpy DT, Cope M, et al. Quantification of cerebral oxygenation and haemodynamics in sick newborn infants by near infrared spectrophotometry. Lancet 1986;4:1063–6.
7. McCormick PW, Stewart M, Goetting MG, et al. Noninvasive cerebral optical spectroscopy for monitoring cerebral oxygen delivery and hemodynamics. Crit Care Med 1991;19:89–97.
8. Kurth CD, Steven JM, Benaron D, Chance B. Near-infrared monitoring of the cerebral circulation. J Clin Monit 1993;9: 163–70.
9. Nioka S, Chance B, Smith DS, et al. Cerebral energy metabolism and oxygen state during hypoxia in neonate and adult dogs. Pediatr Res 1990;28:54–61.
10. Pollard V, Prough DS, DeMelo E, et al. Validation in volunteers of a near-infrared spectroscope for monitoring brain oxygenation in vivo. Anesth Analg 1996;82:269–77.
11. Pollard V, Prough DS, DeMelo E, et al. The influence of carbon dioxide and body position on near-infrared spectroscopic assessment of cerebral hemoglobin oxygen saturation. Anesth Analg 1996;82:278–87.
12. Moskalenko YE, Weinstein GB, Demchenko IT, et al. Biophysical aspects of the cerebral circulation. Oxford: Pergamon Press, 1980.
13. Daubeney PF, Pilkington SN, Janke E, et al. Cerebral oxygenation measured by near-infrared spectroscopy: comparison with jugular bulb oximetry. Ann Thorac Surg 1996;61:930–4.
14. Kurth CD, Liu H, Thayer WS, Chance B. A dynamic phantom brain model for near-infrared spectroscopy. Phys Med Biol 1995;95:2079–92.
15. Chance B, Leigh JS, Miyake H, et al. Comparison of time-resolved and unresolved measurements of deoxyhemoglobin in brain. Proc Natl Acad Sci USA 1988;85:4971–5.
16. Kurth CD, O'Rourke MM, Armstead WM. Validation of time-resolved near-infrared spectroscopy measured cerebral blood volume. J Cereb Blood Flow Metab 1995;15:S616.
17. Sevick EM, Chance B, Leigh J, et al. Quantitation of time and frequency resolved optical spectra for the determination of tissue oxygenation. Anal Biochem 1991;195:330–51.
18. Bland JM, Altman DG. Statistical methods for assessing agreement between two methods of clinical measurement. Lancet 1986;4:307–10.
19. McCormick PW, Stewart M, Goetting MG, Balakrishnan G. Regional cerebrovascular oxygen saturation measured by optical spectroscopy in humans. Stroke 1991;22:596–602.
20. Van der Zee P, Delpy DT. Stimulation of the point spread function for light in tissue by Monte Carlo model: advances in experimental medicine and biology. Adv Exp Med Biol 1987; 215:191–8.
21. Delpy DT, Van der Zee P, Arridge S, et al. Estimation of optical pathlength through tissue from direct time of flight measurement. Phys Med Biol 1988;33:1433–42.
22. Benaron DA, Kurth CD, Steven JM, et al. Transcranial optical path length in infants by near-infrared phase-shift spectroscopy. J Clin Monit 1995;11:109–17.
23. Okada E, Firbank M, Schweiger M, et al. A theoretical and experimental investigation of the effect of sulci on light propagation in brain tissue. Proc IEE Eng Med Biol Soc 1995;12: 1117–9.
24. Rosenthal M, Martel D, LaManna JC, Jobsis FF. In situ studies oxidative energy metabolism during transient cortical ischemia in cats. Exp Neurol 1976;50:477–94.
25. Todd MM, Weeks JB, Warner DS. The influence of intravascular volume expansion on cerebral blood flow and blood volume in normal rats. Anesthesiology 1993;78:945–53.
26. Horecker BL. Absorption spectra of hemoglobin. J Biol Chem 1943;148:173–83.
27. Hazeki O, Tamura M. Quantitative analysis of hemoglobin oxygenation state of rat brain in situ by near-infrared spectrophotometry. J Appl Physiol 1988;64:796–802.
28. Eggert HR, Blazek V. Optical properties of human brain tissue, meninges, and brain tumors in the spectral range of 200 to 900 nm. J Neurosurg 1987;21:459–64.